Int J Clin Exp Med 2017;10(9):13070-13080
www.ijcem.com /ISSN:1940-5901/IJCEM0051721

Original Article

Quantification of MRI-PDFF by complex-based MRI: phantom and rabbit study at 3.0T

Xiaomin Wang[1,2*], Xiaojing Zhang[1*], Lin Ma[1], Shengli Li[3]

[1]Department of Radiology, Chinese PLA General Hospital, Beijing 100853, China; [2]School of Medical Imaging, Tianjin Medical University, Tianjin 300203, China; [3]Laboratory Animal Center, Capital Medical University, Beijing 100069, China. [*]Equal contributors.

Received February 22, 2017; Accepted June 5, 2017; Epub September 15, 2017; Published September 30, 2017

Abstract: This paper aimed to evaluate the accuracy of magnetic resonance imaging-proton density fat fraction (MRI-PDFF) in fat-water-iron phantom and rabbit with hepatic steatosis using complex-based chemical shift-encoded MRI technology. Phantoms of varying fat, water and iron content were constructed. Rabbit model with hepatic steatosis was successfully established by high-fat and high cholesterol diet. All MR examinations were performed on a 3.0T MR system. PDFF values of phantoms and rabbits were calculated from IDEAL-IQ. Fat assessment of rabbit liver biopsy was performed as reference standard. MRI-PDFF of four phantom groups with different iron content has no significant difference with the known fat contents (F=0.011, P=1.0), and extremely close correlations were observed (r=0.998, 0.998, 0.999, 0.998, respectively, all P<0.001). The existence of magnetic microspheres in phantoms did not affect fat measurement accuracy. MRI-PDFF showed significant differences between different steatosis grades with medians of 3.72% (normal), 5.43% (mild), 9.11% (moderate) and 11.17% (severe) except normal with mild steatosis. Close correlation between MRI-PDFF and histological steatosis was observed (r=0.78, P<0.01). IDEAL-IQ provides robust and promising fat quantification and can be considered potential alternative to biopsy for chronic patients where available.

Keywords: MRI, fat quantification, proton density fat fraction (PDFF), phantom, liver

Introduction

Hepatic steatosis (HS) is defined as excessive fat accumulation in hepatocytes. As the earliest manifestation of most common health problems such as nonalcoholic fatty liver disease (NAFLD) [1], steatosis is also considered playing important role in pathogenesis of many hepatic and systemic disorders, and may accelerate disease progression and reduced therapy efficacy [2, 3]. Assessment of liver fat is important for early detection, monitoring and treatment of patients with HS. Biopsy remains gold standard for fat diagnosis, with limitations including invasiveness, sampling bias and subjective variability. Biopsy is not the optimal choice for patients who need long-term clinical follow-up and observations. Among noninvasive surrogates for hepatic steatosis quantification, magnetic resonance (MR) has been confirmed accurate and become a hot spot in clinical researches [4-8].

To date, magnetic resonance imaging-proton density fat fraction (MRI-PDFF) has emerged as a standardized, reproducible and promising biomarker for quantification of hepatic steatosis. It has been a highly active topic and is considered potential alternative to biopsy for chronic patients [9-18].

The multi-echo 3D gradient recalled echo (GRE) sequence named iterative decomposition of water and fat with echo asymmetry and least square estimation (IDEAL-IQ, GE Medical systems, USA), is a complex-based chemical shift encoded MRI quantitative method for diffusive liver diseases in a single breath-hold [9, 19]. Through acquisition of six different echoes, water, fat, in-phase (IP), out-of-phase (OP), R2*, and fat fraction images can be created. PDFF and R2* can be simultaneously obtained by fat fraction and R2* maps to reflect fat and iron content respectively. With simple data processing, IDEAL-IQ has a good prospect of clinical application.

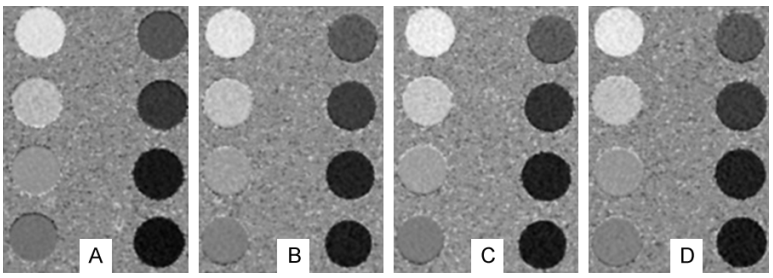

Figure 1. Fat fraction images of phantom groups (known fat volume ratio: first column from top to bottom, 95%, 80%, 65%, 50%; second column from top to bottom, 35%, 20%, 5%, 0%). Each group (A-D) was composed of eight homogeneous fat-water-iron test tubes (20 ml) with different fat volume ratios respectively. SPIO content: (A) None; (B) 0.05 mg; (C) 0.1 mg; (D) 0.15 mg.

Previous clinical researches have shown accurate quantification of hepatic steatosis using IDEAL-IQ [9, 20-23]. Many researches also use IDEAL-IQ to assess fat deposition of different organs of patients [23, 24]. To our knowledge, current state-of-the-art researches on animal model are limited, and researches on efficiency of IDEAL-IQ taking iron influence into account are few in number. This study was aimed to evaluate the accuracy of MRI-PDFF in fat-water-iron phantom and rabbit with hepatic steatosis using IDEAL-IQ. R2* in phantoms was also calculated to investigate efficiency of iron quantification by IDEAL-IQ.

Materials and methods

Phantom construction

In order to test MRI fat quantification in the presence of iron which shortened T2*, phantoms of varying fat, water and iron content were constructed. With similar proton nuclear magnetic resonance (NMR) spectrum to triglyceride, peanut oil was selected [25]. Superparamagnetic iron oxide (SPIO) was applied to investigate influence of iron on fat quantification accuracy of IDEAL-IQ.

According to phantom construction method from Bernard [26], 2 g of carrageenan was dissolved in 400 ml of purified water heated to 50°C by a temperature-controlled magnetic stirrer. 1.8456 g of sodium dodecyl sulfate was added to the solution in order to create homogenous oil-in-water emulsions. Four groups (A, B, C, D) of phantoms (20 ml) were constructed, each of which is composed of eight homogeneous fat-water test tubes with fat volume ratio at 0%, 5%, 20%, 35%, 50%, 65%, 80% and 95% respectively. SPIO content of each phantom group was as follows: A, none; B, 0.05 mg; C, 0.1 mg; D, 0.15 mg. These phantoms were emulsified by a homogenizer to ensure stability of the gels.

Animal model

This work was performed with approval from the Animal Research Committee. Forty New Zealand white rabbits (half male, half female, 2.0-2.5 kg) were randomly divided into four groups: ten rabbits in control group (group G_C) were fed with a standard diet, experimental groups (group G_{E1}, G_{E2}, G_{E3}) were given a high-fat high-cholesterol diet (standard diet with additional 10% lard oil, 2% cholesterol and 5% maltose) for an interval of 4 weeks (group G_{E1}, 4 weeks; G_{E2}, 8 weeks; G_{E3}, 12 weeks) [27, 28].

MRI acquisition

All MRI examinations were performed on a 3.0T MRI system (Discovery MR750 3.0T, GE Medical systems, USA) using an eight-channel phased-array knee coil. IDEAL-IQ sequence was acquired in phantoms and rabbits. Following parameters were chosen: field of view (FOV), 14×14 cm; matrix, 96×96; bandwidth, 100 kHz; flip angle, 5°; slice thickness, 4 mm; repeated measurements (NEX), 3; repetition time (TR), 11.5 ms. The first echo time (TE1)/ΔTE were 1.2/1.9 ms.

Rabbits in the control group (G_C) were divided into three groups to receive MR scanning at different time-points (G_{C1}, 3 rabbits, 4 weeks; G_{C2}, 3 rabbits, 8 weeks; G_{C3}, 4 rabbits, 12 weeks) in order to investigate whether different feeding time affects liver fat content with standard diet, rabbits of each experimental group (G_{E1}, G_{E2} and G_{E3}) underwent MR scanning after different feeding periods. The animals were anaesthetized with intramuscular injection of 0.3 ml xylazine/kg and 0.2 ml raceanisodamine hydrochloride to inhibit stomach and intestine peristalsis, and were immobilized with fixed limbs during MRI examinations. The MRI protocol of rabbits also included routine transverse T2 fast-recovery fast spin-echo (FRFSE) sequence for axial images, and parameters were: FOV,

Table 1. MRI-PDFF of different phantom groups at different known fat volume ratio

Group	MRI-PDFF (%)							
	0%	5%	20%	35%	50%	65%	80%	95%
A	0.54±0.2	3.66±0.9	17.02±1.3	30.41±2.1	44.12±1.3	59.49±1.0	75.29±1.2	93.02±0.7
B	0.84±0.5	4.28±1.0	16.91±0.6	31.40±1.7	49.36±0.9	60.21±1.2	74.39±1.9	94.55±1.1
C	0.60±0.3	3.33±0.6	16.61±1.1	31.58±1.5	45.48±2.7	61.03±0.9	77.00±2.0	93.85±0.8
D	0.86±0.1	4.99±1.2	16.47±2.0	30.40±0.4	49.71±1.6	61.50±2.2	77.92±1.0	95.31±2.2

Values are given as mean ± SD from phantoms in each group.

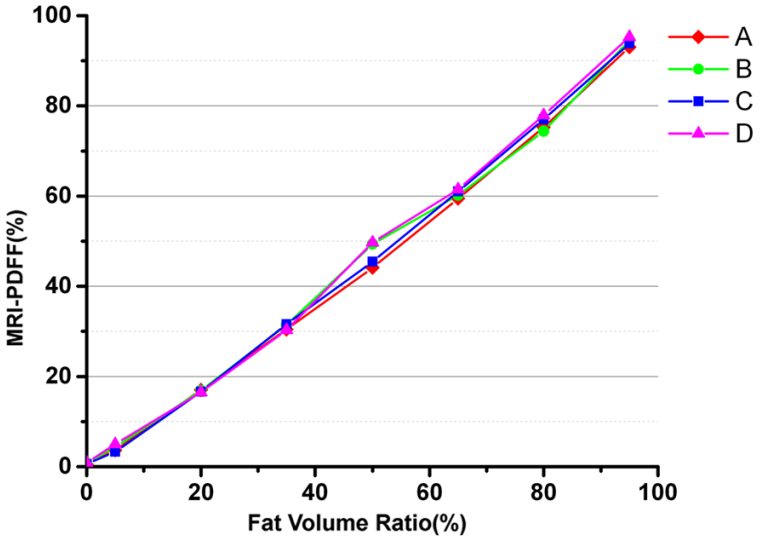

Figure 2. MRI-PDFFs in different phantom groups plotted against known fat volume ratios. No statistically significant differences were observed between MRI-PDFF values of phantom groups (F=0.011, P=1.0) from one-way ANOVA analysis. Pearson correlation measurement showed close correlation between MRI-PDFF and known fat volume ratio in each group, r values were 0.998, 0.998, 0.999 and 0.998 respectively for group A, B, C and D. Each group was composed of eight homogeneous fat-water-iron test tubes (20 ml) with different fat volume ratios respectively. SPIO content: A, none; B, 0.05 mg; C, 0.1 mg; D, 0.15 mg.

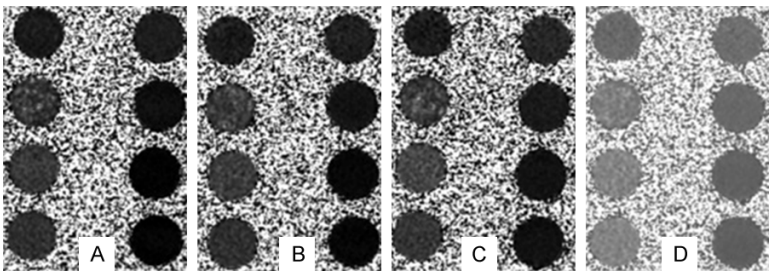

Figure 3. R2* images of phantom groups (known fat volume ratio: first column from top to bottom, 95%, 80%, 65%, 50%; second column from top to bottom, 35%, 20%, 5%, 0%). Each group (A-D) was composed of eight homogeneous fat-water-iron test tubes (20 ml) with different fat volume ratios respectively. SPIO content: (A) None; (B) 0.05 mg; (C) 0.1 mg; (D) 0.15 mg.

12×12 cm; matrix, 256×256; TR, 2861 ms; TE, 68 ms; bandwidth, 41.67 kHz; flip angle, 142°; slice thickness, 4.0 mm; slice spacing, 0.5 mm; NEX, 2.

Data analysis

The radiologist unaware of grouping and biopsy results did data analysis For phantoms, elliptical region of interest (ROI) of 2 cm^2 was placed respectively on fat fraction and R2* image to measure MRI-PDFF and R2*. For rabbits, the radiologist placed five ROIs (average value as measured result) of 0.5 cm^2 on the fat fraction image to measure MRI-PDFF. The selected rabbit images covered the central liver at the level of portal vein. Blood vessels, bile ducts and artifacts should be avoided during ROI placement.

Measurements of the variables were repeated with the interval of a few days to assess calculation reliability. All the calculations were performed on a workstation (AW Volume Share 4; GE Healthcare).

Histological analysis

After MRI imaging, rabbits were deeply anaesthetized and sacrificed by intravenous injection of 5 ml potassium chloride. Liver specimens matching MRI slices to the greatest extent were processed by hematoxylin and eosin (HE) and Oil red O staining to assess the liver morphology and fat

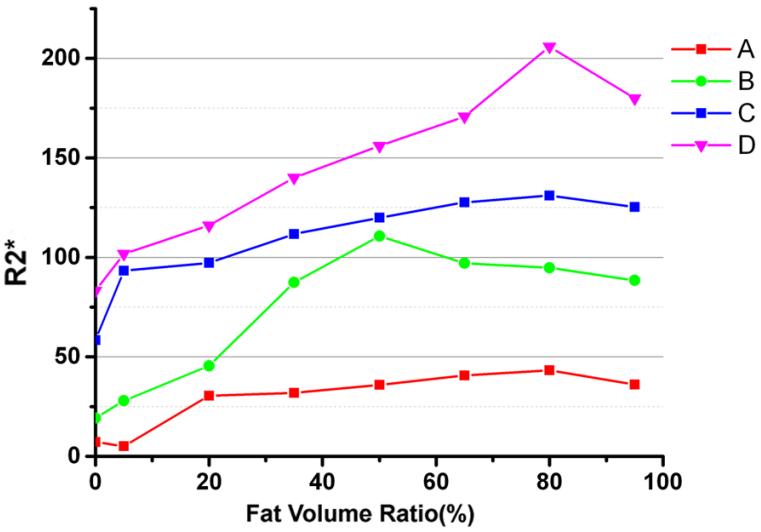

Figure 4. R2*s in different phantom groups plotted against known fat volume ratios. R2* values showed significant differences between phantom groups (F=20.71, P=0.000), however, no correlation between R2* and iron level was observed (P=0.82). Each group (A, B, C, D) was composed of eight homogeneous fat-water-iron test tubes (20 ml) with different fat volume ratios respectively. SPIO content: A, none; B, 0.05 mg; C, 0.1 mg; D, 0.15 mg.

Table 2. Variables measured from rabbit groups with different diets and feeding times

		N	MRI-PDFF (%)	VP (%)
G_C		10	4.27±2.62	8.12±6.17
G_{E1}		9	9.97±3.39	30.43±13.69
G_{E2}		10	8.20±2.24	29.80±7.84
G_{E3}		8	10.18±2.57	42.02±12.12
Overall comparison (χ^2, p)[a]			20.863, 0.000	18.803, 0.000
Multiple comparison (p)[b]	G_C vs G_{E1}		<0.01	<0.01
	G_C vs G_{E2}		<0.01	<0.01
	G_C vs G_{E3}		<0.01	<0.01
	G_{E1} vs G_{E2}		<0.01	>0.05
	G_{E1} vs G_{E3}		>0.05	<0.01
	G_{E2} vs G_{E3}		<0.05	<0.01

Values are given as mean ± SD from phantoms in each group. [a]Kruskal Wallis test; [b]Dunn-Bonferroni test.

droplets in the hepatocytes. According to the nonalcoholic steatohepatitis clinical research network (NASH CRN), hepatic steatosis was graded as following: grade 0, minimal steatosis or normal, <5.0% of liver cells with intracellular vacuoles of fat; grade 1, mild, 5.0%~32.0%; grade 2, moderate, 33.0%~65.0%; grade 3, severe, >65.0% [29]. Semi-automatic quantification (VP) was measured by the ratio of fatty content in liver to liver volume using image analyzer system (Image Pro Plus V6.0). The pathologist blinded to the rabbits' diet and MR values performed biopsy evaluation.

Statistical analysis

Kurtosis and skewness were applied to test the normality of the data distribution. Intraclass correlation coefficient (ICC) was used to assess reliability of IDEAL-IQ calculation. For statistical analysis of phantoms, one-way ANOVA was used to determine whether there were any significant differences between phantom groups in PDFF and R2* values. SNK-Q test performed pairwise comparisons between group values. Pearson correlation measured correlation between measured and known values.

For rabbits, Mann-Whitney U test was used to determine if there was gender difference between male and female rabbits. The comparisons of PDFF and VP among groups or steatosis grades were tested by Kruskal Wallis test followed by Dunn-Bonferroni test for post hoc multiple comparisons. Spearman's correlation coefficient evaluated the degree of association between MRI-PDFF and histological results. All statistical analyses were performed using statistical software (IBM SPSS, version 21.0). *P*<0.05 has statistical significance.

Results

As a measure of reliability, ICC between repeated measurements in IDEAL-IQ PDFF calculations was 0.91 (95% confidence interval [CI]: 0.83-0.95). And ICC between repeated R2* calculation was 0.81 (95% confidence interval [CI]: 0.67-0.90). The measurements of PDFF

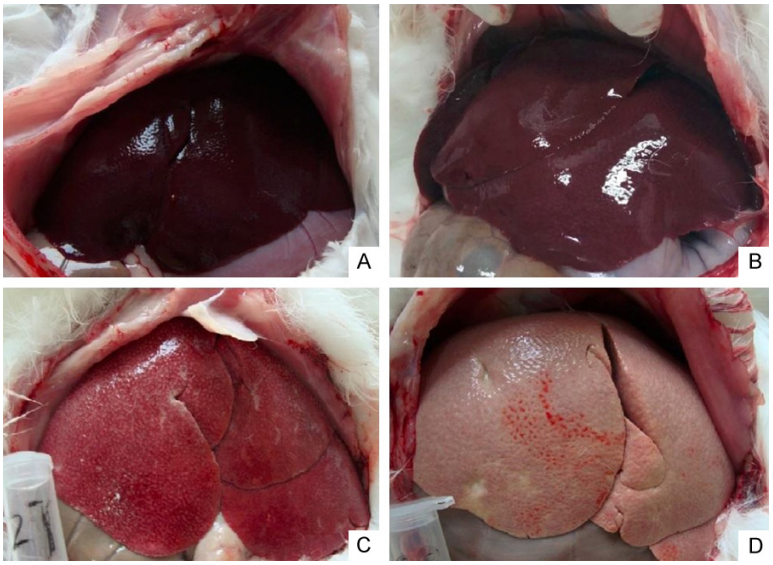

Figure 5. Macroscopic examination of liver with normal (A), mild steatosis (B); moderate steatosis (C) and severe steatosis (D). Normal liver shows red color, smooth surface and sharp margin, while livers with different HS grades were large-sized, dull red to light yellow, rough surfaces with blunt edges and greasy sections.

and R2* from IDEAL-IQ had good repeatability and reliability.

Phantom study

Fat fraction images of different phantom groups were of high quality (**Figure 1**). MRI-PDFF values from IDEAL-IQ of different phantom groups at different known fat volume ratio were showed in **Table 1**. **Figure 2** shows MRI-PDFFs in different phantom groups plotted against known fat volume ratios. One-way ANOVA results indicated no statistically significant differences between MRI-PDFF values of phantom groups (F=0.011, P=1.0). And close correlation between MRI-PDFF and known fat volume ratio was observed in each group, r values were 0.998, 0.998, 0.999 and 0.998 respectively for group A, B, C and D.

R2* values of different phantom groups were also calculated. R2* images were shown in **Figure 3**. Mean R2* values of phantom group A, B, C, D were 28.77±14.62, 71.37±35.00, 108.08±24.38 and 144.22±41.86 (Hz) respectively. R2* values showed significant differences between phantom groups (F=20.71, P=0.000), while no correlation between R2* and iron level was observed (P=0.82). **Figure 4** shows R2*s in different phantom groups plotted against known fat volume ratios.

Animal model study

A total of 37 rabbits (19 male, 18 female) were included in this study (3 died in experimental groups). Rabbits of control group (group G_C) grew well, whereas some rabbits of experimental groups (group G_{E1}, G_{E2}, G_{E3}) showed phenomenon of hair and appetite loss with high-fat high-cholesterol diet.

HS rabbit model was successfully established by high-fat high-cholesterol diet. MRI-PDFFs showed differences between the four groups with different diet and raising period except group G_{E1} and G_{E3}. VPs showed significant differences between each two of the four groups except group G_{E1} and G_{E2} (**Table 2**). And there was no differences in variables between male and female rabbits, *p* values were 0.793, 0.307 respectively in sex comparison of MRI-PDFF and VP.

On the liver biopsy examination, rabbits were divided into different grades as following: 6 (16.2%, 6 from group G_C) with normal liver, 8 (21.6%, 3 from group G_C, 1 from G_{E1}, 2 from G_{E2}, 2 from G_{E3}) with mild steatosis, 13 (35.1%, 1 from group G_C, 2 from G_{E1}, 7 from G_{E2}, 3 from G_{E3}) with moderate steatosis, and 10 (27.1%, 6 from group G_{E1}, 1 from G_{E2}, 3 from G_{E3}) with severe steatosis.

In contrast with liver in the normal group (**Figure 5A**), livers with HS were large-sized, dull red to light yellow, rough surfaces with blunt edges and greasy sections (**Figure 5B-D**). From histology analysis, normal livers did not show any abnormalities in cellular architecture. By contrast, typical histological lesions of steatosis were observed in HS livers. Diffuse severe fatty infiltration was noted in HS livers from HE staining. Fat droplet accumulation and fibrosis were obvious in HS samples stained with Oil red O (**Figure 6**).

Representative T2 weighted, fat fraction and colormap images in normal and HS livers were shown in **Figure 7**. MRI-PDFFs showed signifi-

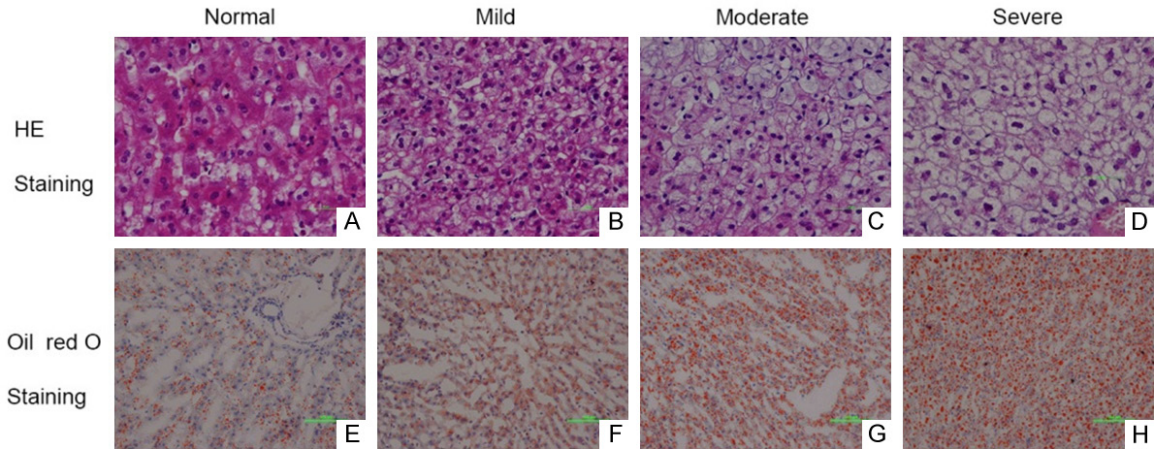

Figure 6. Histologic staining of rabbit liver tissue. The liver specimens were stained with HE (A-D), and Oil red O (E-H). Livers of normal group did not show any abnormalities in cellular architecture, while typical histological lesions of steatosis were observed in HS group. In contrast with normal liver, diffuse severe fatty infiltration was noted in HS group From HE staining. Fat droplet accumulation and fibrosis were obvious in HS samples stained with Oil red O, but not in the normal group.

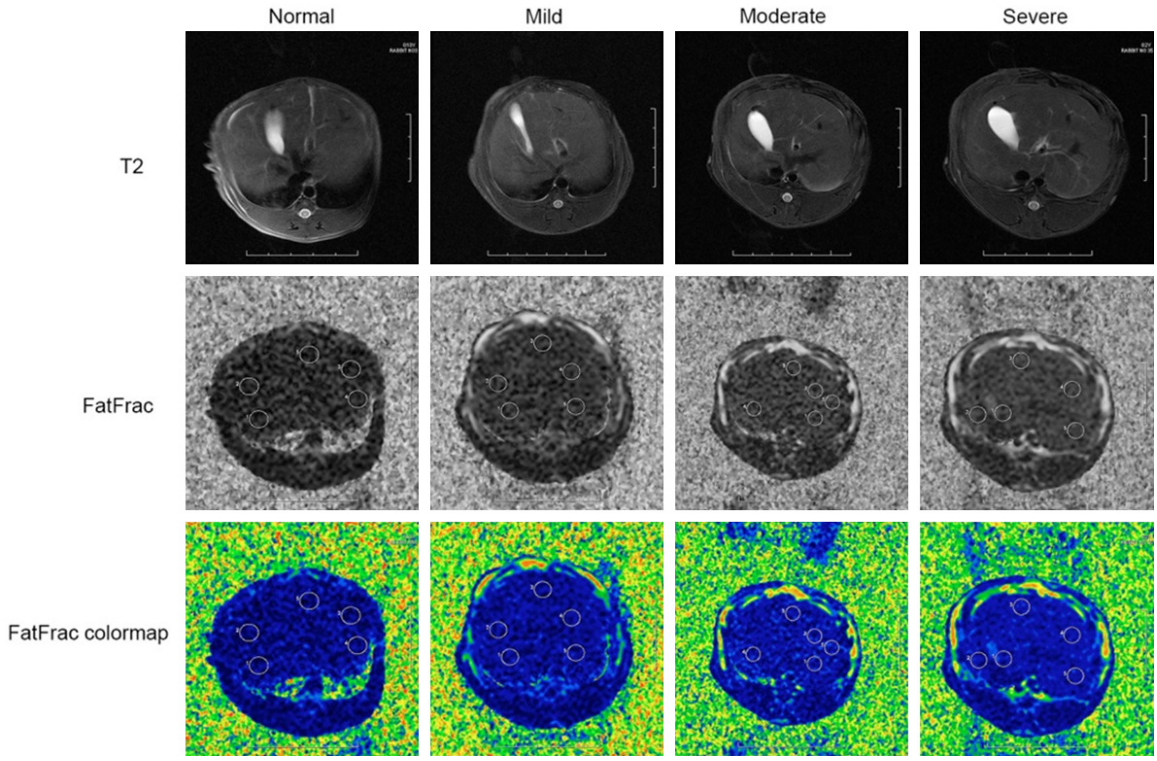

Figure 7. Representative T2 weighted, fat fraction and color map images in normal and HS livers. Five elliptical region of interests (ROIs) of 0.5 cm^2 were placed on the fat fraction and R2* images to measure MRI-PDFF and R2* values.

cant differences among different steatosis grades except normal and mild steatosis. VPs showed significant differences among different steatosis grades (**Table 3**). There was a close correlation between MRI-PDFF and histological VP (r=0.78, P=0.000; **Figure 8**). Scatterplots between VP, MRI-PDFF and histopathologic steatosis grades were shown in **Figure 9**.

Table 3. Liver histology and MRI-PDFF by steatosis grade in rabbits

	Number	MRI-PDFF (%)	VP (%)
Normal (0)	6	3.72±2.36	6.58±3.08
Mild steatosis (1)	8	5.43±2.47	14.51±8.82
Moderate steatosis (2)	13	9.11±2.30	29.10±7.09
Severe steatosis (3)	10	11.17±2.21	46.69±1.74
Overall comparison (x^2, p)[a]		21.634, 0.000	30.043, 0.000
Multiple comparison (p)[b]	0 vs 1	>0.05	<0.05
	0 vs 2	<0.01	<0.01
	0 vs 3	<0.01	<0.01
	1 vs 2	<0.01	<0.01
	1 vs 3	<0.01	<0.01
	2 vs 3	<0.01	<0.01

Values are given as mean ± SD from phantoms in each group. [a]Kruskal Wallis test; [b]Dunn-Bonferroni test.

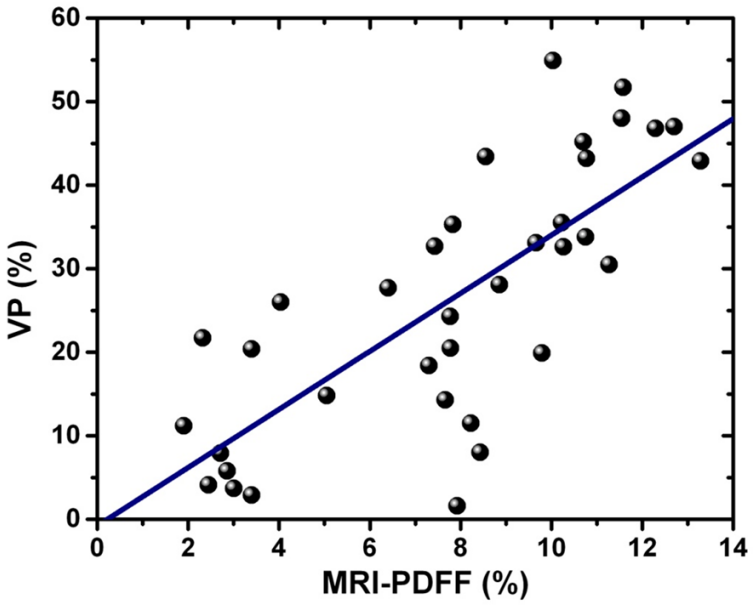

Figure 8. Correlation between Liver MRI-PDFF and VP of histological steatosis. Spearman's correlation analysis showed close correlation between MRI-PDFF and VP (r=0.78, P=0.000).

Discussion

PDFF is defined as accurate separation of fat protons' signal from other protons, proton density becomes the main factor affecting signal strength. T1 bias, T2* decay, spectral complexity of fat, noise bias and eddy currents are the confounding factors in signal acquisition. With correction for these confounders, fat fraction from MRI is equivalent to PDFF [30].

MRI-PDFF has been a robust imaging-based biomarker for hepatic steatosis quantification. Phantom, animal and clinical studies have confirmed accuracy of MRI-PDFF in liver fat quantification and indicated that PDFF is preferred fat quantification where available. Study from Artz demonstrated reproductivity of PDFF across field strengths and methods in obese subjects [31]. Runge compared MRI-PDFF and histopathology against reference standard of biochemically determined liver triglyceride content in mice, and showed that MRI-PDFF (r=0.75) had a higher correlation than histopathology (r=0.59) [32]. MRI-PDFF showed strong correlation with histology (r=0.85) in ex vivo human livers from Bannas [33]. Kukuk compared systematically different methods for hepatic steatosis quantification for patients and confirmed that MRI-PDFF provides the most reliable results [10]. MRI-PDFF has been used as reference or technical standard in many researches [34, 35].

As a complex-based corrected fat quantification technique, IDEAL-IQ uses both magnitude and phase information for accurate separation of fat and water. T1 bias is minimized using a very low flip angle. For correction of T2*, eddy currents and field inhomogeneity (B_0), iteration using magnitude information following complex-based reconstruction was applied in IDEAL-IQ algorithm [19, 24].

With convenient data processing, IDEAL-IQ becomes a hot spot of quantification research. Karcaaltincaba calculated PDFF and R2* using IDEAL-IQ in patients with hepatic iron deposition [36]. Idilman compared the efficiency of MRI-PDFF from IDEAL-IQ in hepatic steatosis quantification in NAFLD patients and observed a close correlation between MRI-PDFF and his-

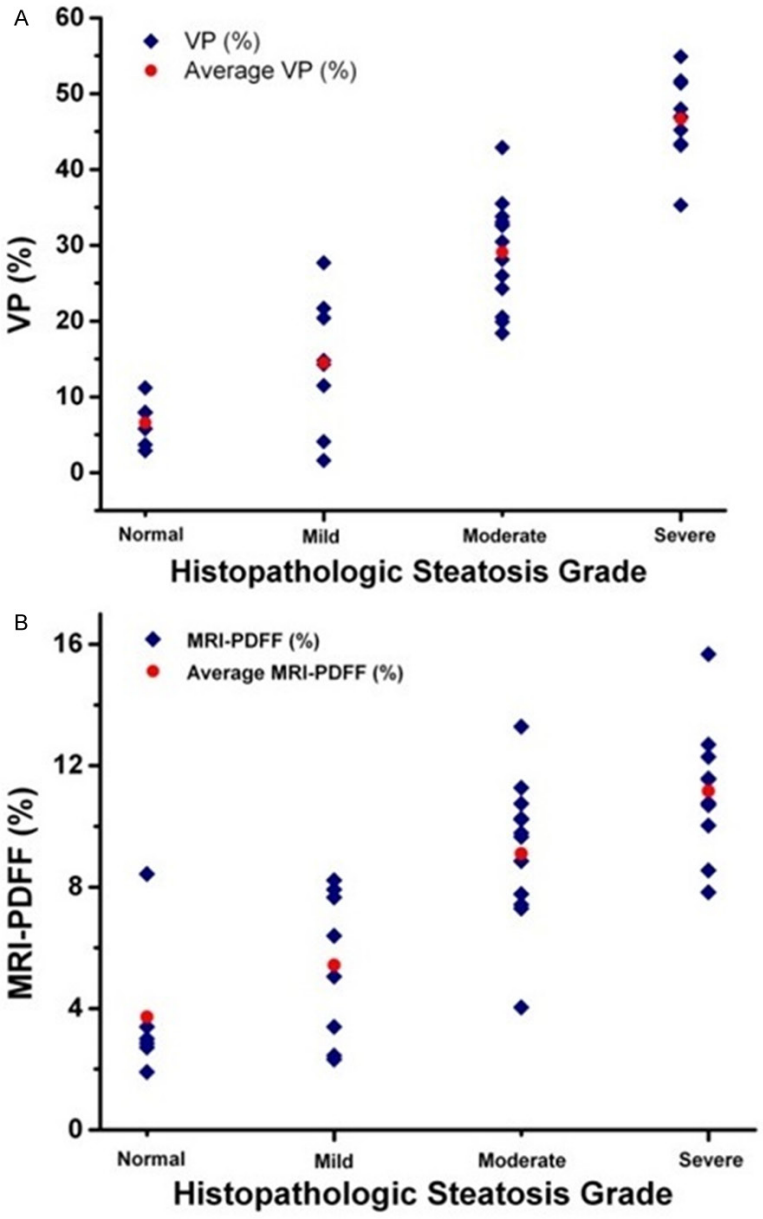

Figure 9. Scatterplots between VP, MRI-PDFF and histologic steatosis grade. The VP and PDFF values increased with the deeper changes of steatosis.

tology (r=0.74, P<0.001) [22]. And in clinical researches, clinical application of IDEAL-IQ was not limited in liver [20, 37].

This study of fat-water-iron phantoms and rabbit model confirmed quantification feasibility and accuracy of IDEAL-IQ in fat research. Evaluated MRI-PDFFs of four phantom groups acquired have no significant difference with the known fat contents, and extremely close correlations were observed (r values were 0.998, 0.998, 0.999, 0.998). The existence of magnetic microspheres in phantoms did not affect fat measurement accuracy. Rabbit study showed that MRI-PDFF was significantly different between hepatic steatosis grades except normal and mild steatosis, and had close correlation with histological results. Nevertheless, the threshold determination of different steatosis grades and sensitivity of mild steatosis from IDEAL-IQ needs further study.

R2* calculation was also performed in fat-water-iron phantoms, and showed significant differences between different SPIO contents. Nevertheless, no correlation between R2* and iron level was observed. The R2* distribution in phantoms (**Figure 4**) showed differences between varying iron contents at specific fat content. Based on gradient echo acquisitions, R2* is calculated from exponential signal decay rate. Signal model, fat correction and B_0 field variations are critical for estimation of R2* values. R2* measurements with relevant confounding factors corrected have shown to be efficiency in iron evaluation. Liau evaluated performance of MRI-PDFF and R2* in liver and spine by intravenous infusion of superparamagnetic iron oxide (SPIO) contrast, and confirmed that IDEAL-IQ is robust to R2* evaluation [38]. But R2* does not measure iron content directly, and spatial variability of iron concentration lead to broad quantification confidence intervals. With respect to hepatic R2*-based iron evaluation, coexisting conditions such as fat, inflammation and fibrosis must be taken into account. From the results of phantoms, R2* value was affected by fat content, R2* values with same iron content fluctuate at different fat contents. Further studies to evaluate the efficiency of R2* from IDEAL-IQ are needed.

Accurate quantification of liver fat is critical for clinical diagnosis and treatment of important hepatic and systemic disorders, and facilitates research on related fields. The continuous development of MRI technologies, particularly the accomplishment of IDEAL-IQ measuring MRI-PDFF and R2* simultaneously, has provided prominent measures for diagnosis and quantification of steatosis and iron deposition, especially for patients who need long-term clinical follow-up and observations.

From this phantom and rabbit research, IDEAL-IQ provides robust and promising fat quantification and can be considered potential alternative to biopsy for chronic patients where available. Evaluations of the reliability and accuracy of the technology are still critical in order to determine whether they can substitute histological examination as the gold standard to assess hepatic steatosis deposition. R2* from IDEAL-IQ is sensitive to iron changes, however, R2* measurement and classification for iron deposition using IDEAL-IQ need further experimental investigation.

Disclosure of conflict of interest

None.

Address correspondence to: Dr. Lin Ma, Department of Radiology, Chinese PLA General Hospital, 28 Fuxing Road, Beijing 100853, China. Tel: +86-13801222069; Fax: +86-10-66939592; E-mail: cjr.malin@vip.163.com

References

[1] Fabbrini E and Magkos F. Hepatic steatosis as a marker of metabolic dysfunction. Nutrients 2015; 7: 4995-5019.

[2] Lok AS, Everhart JE, Chung RT, Kim HY, Everson GT, Hoefs JC, Greenson JK, Sterling RK, Lindsay KL, Lee WM, Di Bisceglie AM, Bonkovsky HL, Ghany MG and Morishima C. Evolution of hepatic steatosis in patients with advanced hepatitis C: results from the hepatitis C antiviral long-term treatment against cirrhosis (HALT-C) trial. Hepatology 2009; 49: 1828-1837.

[3] Tarantino G. Pathogenesis of hepatic steatosis: the link between hypercortisolism and non-alcoholic fatty liver disease. World J Gastroenterol 2013; 19: 6735.

[4] Goceri E, Shah ZK, Layman R, Jiang X and Gurcan MN. Quantification of liver fat: a comprehensive review. Comput Biol Med 2016; 71: 174-189.

[5] Ligabue G, Besutti G, Scaglioni R, Stentarelli C and Guaraldi G. MR quantitative biomarkers of non-alcoholic fatty liver disease: technical evolutions and future trends. Quant Imaging Med Surg 2013; 3: 192-195.

[6] Reeder SB, Cruite I, Hamilton G and Sirlin CB. Quantitative assessment of liver fat with magnetic resonance imaging and spectroscopy. J Magn Reson Imaging 2011; 34: 729-749.

[7] Sharma P, Altbach M, Galons JP, Kalb B and Martin DR. Measurement of liver fat fraction and iron with MRI and MR spectroscopy techniques. Diagn Interv Radiol 2014; 20: 17-26.

[8] Yokoo T, Browning JD. <Fat and iron quantification in the liver past, present, and future>. Top Magn Reson Imaging 2014; 23: 73-94.

[9] Idilman IS, Aniktar H, Idilman R, Kabacam G, Savas B, Elhan A, Celik A, Bahar K, Karcaaltincaba M. Hepatic steatosis: quantification by proton density fat fraction with MR imaging versus liver biopsy. Radiology 2013; 3: 767-775.

[10] Kukuk GM, Hittatiya K, Sprinkart AM, Eggers H, Gieseke J, Block W, Moeller P, Willinek WA, Spengler U, Trebicka J, Fischer HP, Schild HH and Traber F. Comparison between modified Dixon MRI techniques, MR spectroscopic relaxometry, and different histologic quantification methods in the assessment of hepatic steatosis. Eur Radiol 2015; 25: 2869-2879.

[11] Leiber LM, Boursier J, Michalak S, Roullier V, Fizanne L, Chaigneau J, Roux J, Moal V, Flamment M, Bazeries P, Ducluzeau PH and Aube C. MRI versus histological methods for time course monitoring of steatosis amount in a murine model of NAFLD. Diagn Interv Imaging 2015; 96: 915-922.

[12] Leporq B, Lambert SA, Ronot M, Boucenna I, Colinart P, Cauchy F, Vilgrain V, Paradis V and Van Beers BE. Hepatic fat fraction and visceral adipose tissue fatty acid composition in mice: quantification with 7.0T MRI. Magn Reson Med 2016; 76: 510-518.

[13] Noureddin M, Lam J, Peterson MR, Middleton M, Hamilton G, Le TA, Bettencourt R, Changchien C, Brenner DA, Sirlin C and Loomba R. Utility of magnetic resonance imaging versus histology for quantifying changes in liver fat in nonalcoholic fatty liver disease trials. Hepatology 2013; 58: 1930-1940.

[14] Rehm JL, Wolfgram PM, Hernando D, Eickhoff JC, Allen DB and Reeder SB. Proton density fat-fraction is an accurate biomarker of hepatic steatosis in adolescent girls and young women. Eur Radiol 2015; 25: 2921-2930.

[15] Tang A, Desai A, Hamilton G, Wolfson T, Gamst A, Lam J, Clark L, Hooker J, Chavez T, Ang BD, Middleton MS, Peterson M, Loomba R and Sirlin CB. Accuracy of MR imaging-estimated

proton density fat fraction for classification of dichotomized histologic steatosis grades in nonalcoholic fatty liver disease. Radiology 2014; 2: 416-425.
[16] Zand KA, Shah A, Heba E, Wolfson T, Hamilton G, Lam J, Chen J, Hooker JC, Gamst AC, Middleton MS, Schwimmer JB and Sirlin CB. Accuracy of multiecho magnitude-based MRI (M-MRI) for estimation of hepatic proton density fat fraction (PDFF) in children. J Magn Reson Imaging 2015; 42: 1223-1232.
[17] Lin SC, Heba E, Bettencourt R, Lin GY, Valasek MA, Lunde O, Hamilton G, Sirlin CB and Loomba R. Assessment of treatment response in non-alcoholic steatohepatitis using advanced magnetic resonance imaging. Aliment Pharmacol Ther 2017; 45: 844-854.
[18] Imajo K, Kessoku T, Honda Y, Tomeno W, Ogawa Y, Mawatari H, Fujita K, Yoneda M, Taguri M, Hyogo H, Sumida Y, Ono M, Eguchi Y, Inoue T, Yamanaka T, Wada K, Saito S and Nakajima A. Magnetic resonance imaging more accurately classifies steatosis and fibrosis in patients with nonalcoholic fatty liver disease than transient elastography. Gastroenterology 2016; 150: 626-637, e627.
[19] Reeder SB, Robson PM, Yu H, Shimakawa A, Hines CD, McKenzie CA and Brittain JH. Quantification of hepatic steatosis with MRI: the effects of accurate fat spectral modeling. J Magn Reson Imaging 2009; 29: 1332-1339.
[20] Aoki T, Yamaguchi S, Kinoshita S, Hayashida Y and Korogi Y. Quantification of bone marrow fat content using iterative decomposition of water and fat with echo asymmetry and least-squares estimation (IDEAL): reproducibility, site variation, and correlation with age and menopause. Br J Radiol 2016; 89: 20120538.
[21] Ge M, Zhang J, Wu B, Liu Z, Song H, Meng X and Wu X. Effect of gadolinium on hepatic fat quantification using multi-echo reconstruction technique with T2* correction and estimation. Eur Radiol 2016; 26: 1913-1920.
[22] Idilman IS, Keskin O, Celik A, Savas B, Halil Elhan A, Idilman R and Karcaaltincaba M. A comparison of liver fat content as determined by magnetic resonance imaging-proton density fat fraction and MRS versus liver histology in non-alcoholic fatty liver disease. Acta Radiol 2016; 57: 271-278.
[23] Meng X, Chen X, Shen Y, Hu X, Tang H, Hu D, Li Z and Kamel IR. Proton-density fat fraction measurement: a viable quantitative biomarker for differentiating adrenal adenomas from nonadenomas. Eur J Radiol 2017; 86: 112-118.
[24] Idilman IS, Tuzun A, Savas B, Elhan AH, Celik A, Idilman R and Karcaaltincaba M. Quantification of liver, pancreas, kidney, and vertebral body MRI-PDFF in non-alcoholic fatty liver disease. Abdom Imaging 2015; 40: 1512-1519.
[25] Hines CD, Yu H, Shimakawa A, McKenzie CA, Brittain JH and Reeder SB. T1 independent, T2* corrected MRI with accurate spectral modeling for quantification of fat: validation in a fat-water-SPIO phantom. J Magn Reson Imaging 2009; 30: 1215-1222.
[26] Bernard CP, Liney GP, Manton DJ, Turnbull LW and Langton CM. Comparison of fat quantification methods: a phantom study at 3.0T. J Magn Reson Imaging 2008; 27: 192-197.
[27] Hebbard L and George J. Animal models of nonalcoholic fatty liver disease. Nat Rev Gastroenterol Hepatol 2011; 8: 35-44.
[28] King JL, Miller RJ, Blue JP, O'Brien WD and Erdman JW. Inadequate dietary magnesium intake increases atherosclerotic plaque development in rabbits. Nutr Res 2009; 29: 343-349.
[29] Joo I, Lee MJ, Yoon JH, Jang JJ, Han JK and Choi BI. Nonalcoholic fatty liver disease: intravoxel incoherent motion diffusion-weighted MR imaging-an experimental study in a rabbit model. Radiology 2013; 270: 131-140.
[30] Reeder SB and Sirlin CB. Quantification of liver fat with magnetic resonance imaging. Magn Reson Imaging Clin N Am 2010; 18: 337-357, ix.
[31] Artz NS, Haufe WM, Hooker CA, Hamilton G, Wolfson T, Campos GM, Gamst AC, Schwimmer JB, Sirlin CB and Reeder SB. Reproducibility of MR-based liver fat quantification across field strength: same-day comparison between 1.5T and 3T in obese subjects. J Magn Reson Imaging 2015; 42: 811-817.
[32] Runge JH, Bakker PJ, Gaemers IC, Verheij J, Hakvoort TB, Ottenhoff R, Nederveen AJ and Stoker J. Measuring liver triglyceride content in mice: non-invasive magnetic resonance methods as an alternative to histopathology. MAGMA 2014; 27: 317-327.
[33] Bannas P, Kramer H, Hernando D, Agni R, Cunningham AM, Mandal R, Motosugi U, Sharma SD, Munoz del Rio A, Fernandez L and Reeder SB. Quantitative magnetic resonance imaging of hepatic steatosis: validation in ex vivo human livers. Hepatology 2015; 62: 1444-1455.
[34] Lin SC, Heba E, Wolfson T, Ang B, Gamst A, Han A, Erdman JW Jr, O'Brien WD Jr, Andre MP, Sirlin CB and Loomba R. Noninvasive diagnosis of nonalcoholic fatty liver disease and quantification of liver fat using a new quantitative ultrasound technique. Clin Gastroenterol Hepatol 2015; 13: 1337-1345, e1336.
[35] Hur BR, Lee JM, Hyunsik W, Lee KB, Joo I, Han JK and Choi BI. Quantification of the fat frac-

tion in the liver using dual-energy computed tomography and multimaterial decomposition. J Comput Assist Tomogr 2014; 38: 845-852.

[36] Karcaaltincaba M, Idilman I and Celik A. Focal sparing of iron and fat in liver tissue in patients with hemosiderosis: diagnosis with combination of R2* relaxometry and proton density fat fraction calculation by MRI. Diagn Interv Radiol 2011; 17: 323-327.

[37] Grayev A, Reeder S and Hanna A. Use of chemical shift encoded magnetic resonance imaging (CSE-MRI) for high resolution fat-suppressed imaging of the brachial and lumbosacral plexuses. Eur J Radiol 2016; 85: 1199-1207.

[38] Liau J, Shiehmorteza M, Girard OM, Sirlin CB and Bydder M. Evaluation of MRI fat fraction in the liver and spine pre and post SPIO infusion. Magn Reson Imaging 2013; 31: 1012-1016.